Available online at www.sciencedirect.com
ScienceDirect
Ceramics International 33 (2007) 1275–1282
CERAMICS INTERNATIONAL
www.elsevier.com/locate/ceramint

Synthesis and characterization of sol–gel derived ZrO_2 doped Al_2O_3 nanopowder

Debasish Sarkar [a,*], Deepak Mohapatra [a], Sambarta Ray [a], Santanu Bhattacharyya [a], Sukumar Adak [a], Niren Mitra [b]

[a] Department of Ceramic Engineering, National Institute of Technology, Rourkela-8, Orissa, India
[b] Department of Chemical Technology, University of Calcutta, 92, APC Road, Kolkata-9, India

Received 30 November 2005; received in revised form 23 February 2006; accepted 2 May 2006
Available online 12 September 2006

Abstract

Al_2O_3–ZrO_2 composite gel precursor powder containing 5–15 mol% ZrO_2 was prepared by wet chemical route. The washed gel containing pseudoboehmite and amorphous zirconia was characterized with respect to DTA/TG, XRD and IR spectroscopy. The DTA/TG result indicates three-stage decomposition for pseudoboehmite and single stage decomposition for amorphous zirconia. In the calcined powder phase evolution of Al_2O_3 follows the sequence pseudoboehmite → bayerite → boehmite → γ-Al_2O_3 → θ-Al_2O_3 → α-Al_2O_3, while that of ZrO_2 follows amorphous ZrO_2 → t-ZrO_2 → (t + m)ZrO_2. FTIR studies revealed that the number of M–OH and M–O bond increase on increasing mol% of ZrO_2 due to a change in the cationic charge of the composite powder. TEM photograph of calcined powder showed both dispersed nano-size spherical particle as well as agglomerated particles. EPMA confirmed the near uniform distribution of zirconia particles in the alumina matrix.

Keywords: Alumina–zirconia; Hydrogel; Crystallization; FTIR; TEM

1. Introduction

Alumina is one of the most widely used structural ceramics [1,2]. Several properties of alumina are controlled by its microstructure and its matrix stability. Moreover, additive interactions can modify and achieve tailor made properties of alumina ceramics. Zirconia is one such additive which can increase the strength and toughness of alumina matrix either by stress-induced transformation toughening or by microcrack toughening [3]. The extent of stress-induced transformation toughening depends on the dispersion of tetragonal zirconia (t-ZrO_2) in alumina matrix, its volume fraction and transformability. On the other hand, a uniform distribution of ZrO_2 in ceramic matrix is an important factor for optimization of microcrack nucleation-induced toughening [4,5]. The uniform dispersion of zirconia particles in the alumina matrix can be controlled by homogeneous powder synthesis techniques. A series of powder processing techniques have been investigated to synthesize homogenous powder mixture and amongst them the precipitation and the sol–gel methods are the easy and commercialized chemical synthesis routes for producing zirconia doped nanoparticles [6–10].

The zirconium hydroxide obtained through sol–gel or precipitation route could be represented by $ZrO_2{\cdot}nH_2O$ or $ZrO(OH)_n$ showing that Zr has a higher coordination number in the hydrated state in comparison to unhydrated oxide states [11]. The presence of more than one structure of zirconium hydroxide suggests that Zr forms different inorganic polymers with bridged hydroxyl groups. The final gel precursor structure, however, is dependent on the monomer structure during the progress of polymerization [12].

Recently, Caracoche et al. synthesized nano-zirconia powders using the sol–gel method through pH control of the precursor solution [13]. Chen et al. also observed that in the pH range 7–10.5, the predominant monomer cluster is $[Zr(OH)_6]^{2-}$ (Fig. 1a), which preferentially produces tetragonal (t) precursor structure with slow alkali addition (Fig. 1b) [14]. Therefore, the bonding mechanisms of Zr–OH and its final phase content depend on bridging hydroxyl groups, monomer structure, polymerization kinetics and pH of the precursor solution.

* Corresponding author. Tel.: +91 661 2462207; fax: +91 661 2462999.
E-mail address: dsarkar@nitrkl.ac.in (D. Sarkar).

0272-8842/$32.00
doi:10.1016/j.ceramint.2006.05.002

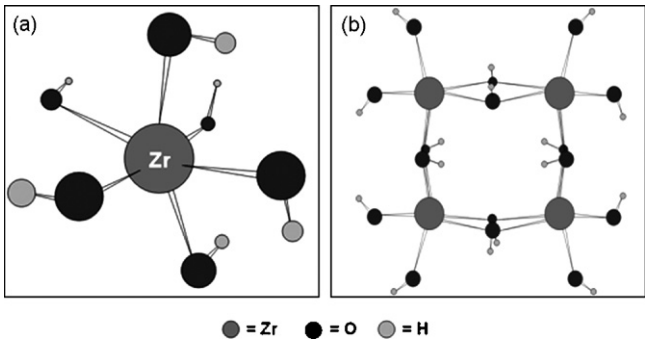

Fig. 1. Cluster structure of $[Zr(OH_6]^{2-}$ (a) and ordered structure of polymerization precursors (b).

The synthesis of ZrO_2 dispersed Al_2O_3 precursor powders from multiphase hydrogel is a complex subject, which depends on the configuration of hydroxide of Al and Zr and its polymerization. The chemistry and polymerization of aluminum oxide and hydroxide depend on acid/base properties. The proton activity is significantly affected by the oxygen coordination surrounding Al^{3+}. In the deprotonated form of the aluminum hydroxide in water $[Al(OH)_4]^-$, Al atom is tetrahedrally coordinated with oxygen atoms, whereas all the protonated cationic species in the series $Al(OH)^{2+}$(aq) to Al^{3+}(aq) are six-coordinated. This amphoteric nature of $Al(OH)_3$ in water is the cause for the stability of hydrogel [15]. Zakharchenya and Vasilevskaya investigated the influence of temperature on the dehydration and crystallization behavior of such stable hydrogel products [16].

The above discussion summarizes that the phase evolution sequence during crystallization of alumina–zirconia from its hydrated precursor depend among other factors on the nature and type of bonding present in the hydroxides of Al and Zr. Particularly for ZrO_2, the processing route can alter the nature of bonds in the Zr hydroxide monomer [14]. The monomer type in turn influences the phases formed in ZrO_2. As a result the detailed study of bond type of Al and Zr hydroxide becomes important for predicting the final phase mixture of alumina–zirconia composite powder. FTIR is a very sensitive and well-established tool for studying the orientation, transformation and nature of hydroxyl bonds in both Al and Zr hydrogel. The position and intensity of the IR peaks are also strongly influenced by the crystallization behavior, degree of crystallinity, morphology and particle size. Therefore, the FTIR results could well be correlated with the crystallization behavior and phase evolution in the gel as well as calcined powder in zirconia dispersed alumina system. Hence, the present research discusses crystallization behavior and phase evolution of ZrO_2 dispersed Al_2O_3 nanopowder (having varying proportion of ZrO_2) prepared from a complex hydrogel. The present study also includes the detailed FTIR analysis of the hydrogel as well as calcined powder and correlates the FTIR results with that of thermal analysis and XRD.

2. Experimental

Aluminum nitrate (E-Merck, India) and zirconium oxychloride (E-Merck, India) were used as precursor for preparing high alumina–zirconia composite powder. Solutions of aluminum nitrate (0.5 M) and zirconium oxychloride (0.5 M) were mixed together in the required proportions to yield different Al_2O_3–$x$$ZrO_2$ (where $x = 5$, 7.5, 10 and 15 mol%) batches. The mixed hydrogel was obtained by drop wise addition of 1:1 NH_3 hydroxide solution into the continuously stirred mixed aqueous solution of Al and Zr salt maintained at 25 °C. The viscosity of the batch gradually increased and finally set to an enblock gel at pH ~9. The gels were then aged at room temperature for 48 h. Subsequently, the gel of each composition was washed repeatedly with boiling distilled water to remove chloride and nitrate ions and filtered. The filter cake was oven dried. The dried gels were calcined in air in a muffle furnace at different temperatures varying from 200 to 1400 °C with a hold time of 2 h at the corresponding peak temperatures. The composition of each batch has been listed in Table 1.

For phase analysis, X-ray diffraction study of the dried gel and calcined powders were carried out in a Philips X-ray diffractometer (PHILIPS PW1830), using Cu Kα radiation. The voltage and current setting were 35 kV and 30 mA, respectively. The samples were continuously scanned with a step size of 0.02° (2θ) and a count time of 1 s per step. Silicon was used as an internal standard. The crystallite size of the synthesized powder was determined from X-ray line broadening using the Scherrer's equation as follows:

$$D = \frac{0.9\lambda}{B\cos\theta} \quad (1)$$

where D is the crystallite size (nm), λ the wavelength of the X-ray radiation (1.54056 Å), θ the Bragg's angle and B is the full width at half maximum (FWHM), where $B = (B^2_{meas} - B^2_{equip})^{1/2}$. B_{meas} = measured FWHM and B_{equip} = FWHM due to instrumental broadening.

The thermal decomposition behavior of the washed and dried gel was studied by TG–DTA analysis (Netzsch STA 409C) upto 1200 °C at a heating rate of 10 °C/min. The particle size of the calcined Al_2O_3–15 mol% ZrO_2 (A15Z) powder was characterized by TEM (JEM 2000 FX). The particle size distribution (vol.%) of the calcined powder was carried out using laser particle size analyzer (Malvern, Mastersizer 2000, UK). Surface area of the as-dried gel powder was carried out by nitrogen adsorption using BET surface area analyzer (Quantachrome, USA). FTIR analysis of dried gel and calcined powders were carried out in a DRIFT Magna IR560, Nicolet spectrometer in the wavenumber range 400–4000 cm^{-1} at resolution of 4 cm^{-1} for studying the chemical groups on the surface of the as-dried gel as well as calcined powder. A small amount of sample (0.2 g) was thoroughly mixed with ground

Table 1
Composition of the gel precursor

Identification	Al_2O_3 (mol%)	ZrO_2 (mol%)
A5Z	95	5
A75Z	92.5	7.5
A10Z	90	10
A15Z	85	15

KBr in an agate mortar and a disc was prepared in vacuum maintaining a pressure of 33 kg/cm^2.

The distribution of Al_2O_3 and ZrO_2 was observed on the sintered sample (1600 °C/4 h) using an electron probe microanalysis (EPMA JEOL-JXA8600). The samples were polished, thermally etched (1500 °C for 30 min) and gold coated before observation.

3. Results and discussions

3.1. FTIR analysis

The major peaks appearing in the FTIR spectra of alumina–zirconia hydroxide system could be related to the following:

(1) –OH stretching vibration of the surface bonded or adsorbed water;
(2) –OH bending vibration of the surface bonded or adsorbed water;
(3) –OH stretching vibration of structural water, corresponding to M–OH bonding;
(4) –OH bending vibration of structural water, corresponding to M–OH bonding;
(5) Al–O stretching vibration;
(6) Zr–O stretching vibration.

The IR spectral frequency of uncalcined hydrogels and calcined powders of all the compositions are presented in Table 2 and the detailed IR spectra of the A15Z powder calcined at different temperatures have been shown in Fig. 2. All the gels and calcined samples exhibited –OH *stretching vibration* in the frequency range of 3136–3857 cm^{-1}. The reduced reflectance and bond depth of the gel powder could be ascribed to the non-crystalline nature of the material [17]. The number of peaks for –OH stretching vibration in the Al_2O_3–ZrO_2 powder increases with an increase in the ZrO_2 content. The increased IR interaction probably reflects a gradual change in the composition and heterogeneity in the bond as well as a switchover from a homogenous single phase structure to a homogenous two phase structure intuitive.

The frequency of different vibrational modes of Al–OH and/or Zr–OH including the bending and stretching modes are altered due to change in the charge distribution among molecules. This altered frequency of vibration in turn causes a change in the electrical dipole moment of the original species. The charge distribution around each Al–OH and/or Zr–OH and associated vibration is influenced by the charge on its neighboring species. Hence, the continuum vibration of the matrix is responsible for the change in dipole moment and establishment of an electric field of the composite powder. The increased cationic charge in the alumina–zirconia composite powder due to the introduction of Zr^{4+} interacts strongly with the polar inner hydroxyl groups. This interaction probably results in the reduction of vibrational dipole moment in bending thereby creating a greater force of attraction (antisymmetric coupling) on the stretching vibration.

Table 2
IR spectral frequency (cm^{-1}) of Al_2O_3–ZrO_2 systems with respect to temperatures

Material	Dried gel	200 °C	400 °C	1000 °C
A5Z	3656.2	3657.1	3461	3484.3
	3553.3	3620.7		
	3471.8	3553.2		
	3146.2	3466.9		
		3141.6		
	2365.7	2396.1	2371.4	
	2089.9	2065.6		1643.7
	1762.0	1762.7	1636.6	1395.9
	1629.7	1632.6	1384.7	
	1383.9	1384.8		
	1070.8	1025.6		
	978.7	978.2		839.8
	767.7	765.9	596.7	537.4
	515.8	526.9		
A75Z	3656.3		3449.2	3484.3
	3553.3			
	3468.9			
	3140.8			
	2396.8		2368.1	
	2065.5			
	1763.0		1637.8	1642.3
	1630.9		1385.5	1425.3
	1387.3			
	978.7			846.2
	767.0		582.2	542.3
	523.2			
A10S	3656.5	3465.5		3484.3
	3552.3	3144.0		
	3472.5			
	3139.3			
	2396.2	2369.0		
	2065.7			
	1763.0	1629.6		1641.2
	1631.8	1380.6		
	1385.2			
	1070.4	1065.5		832.8
	977.0			
	760.5	767.9		568.0
	514.3	523.8		
A15S	3857.5	3447.9	3449.9	3450.8
	3656.4			
	3552.0			
	3471.5			
	3425.8			
	3136.0			
	2396.6	2361.7	2371.8	
	2066.3			
	1763.1	1638.2	1636.2	1629.5
	1634.8	1385.3	1385.4	
	1385.0			
	1069.6	667.9		828.0
	977.1			
	825.3			
	762.8		585.3	525.6
	515.6			

The stretching vibration for structural –OH and adsorbed water appear at wave number greater than 3000 cm^{-1} for all the AZ compositions. A careful inspection of stretching frequencies reveal that an increase in ZrO_2 content in the batch causes a significant change in the –OH stretching pattern upto 10% ZrO_2

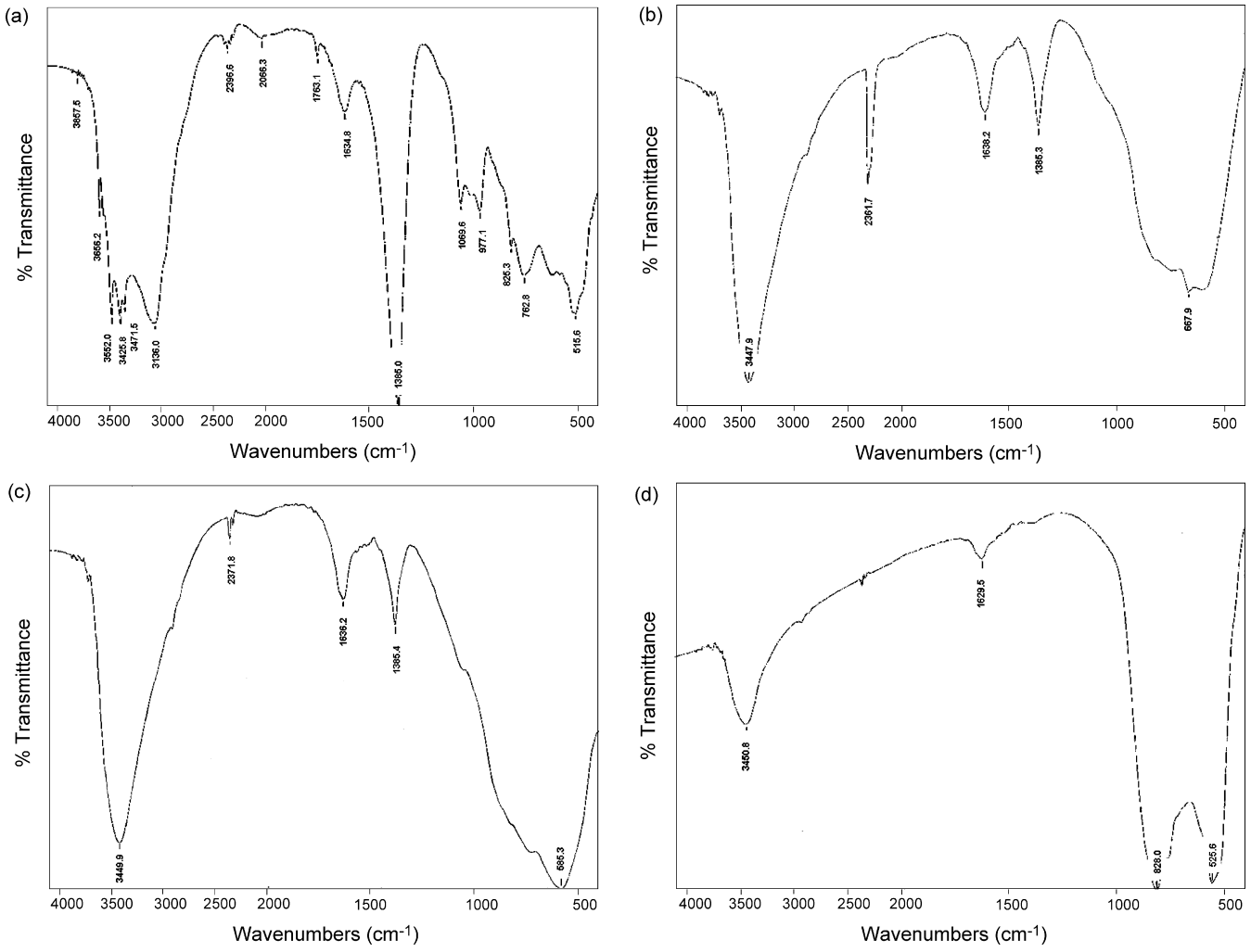

Fig. 2. FTIR curves of Al_2O_3–$15ZrO_2$ (mol%): (a) dried gel, (b) 200 °C, (c) 400 °C and (d) 1000 °C.

addition for A5Z to A10Z samples. Four peaks are observed in the wave number range 3656, 3553, 3471 and 3146 cm^{-1} which account for –OH stretching. In the A15Z samples two more additional peaks appear at 3857 and 3425 cm^{-1} (Fig. 2a), which indicate the presence of more –OH in this batch. These two additional vibrations are probably due to –OH groups attached to the Zr^{4+}.

For all AZ samples the vibrations appearing in the range 2396 and 2065 cm^{-1} could be assigned to the coupling effect of *stretching and bending vibrations* of –OH groups. The peaks which appear at 1764, 1634 and 1385 cm^{-1} are due to the *bending vibration* of Zr–OH groups. The peak positions are more or less the same in all the samples. The peaks between 1070 and 760 cm^{-1} correspond to *Al–O vibration* [18]. The strong absorption band of the latter one may be attributed to six-coordinated Al^{3+} ions. These O–H and Al–O vibrations are characteristics of pseudoboehmite. The absorption band at 1070 cm^{-1} is due to the presence of alumina gel. The above results conclude that alumina in this particular alumina–zirconia system is present as an intermediate bayerite. The –OH stretching and bending vibrations is exhibited by both the constituents of the hydrogels. The absorption bands at 514–523 cm^{-1} correspond to *Zr–O vibrations*.

A5Z samples calcined at 200 °C shows an additional peak at 3620.7 cm^{-1}(Table 3). This is related to the activation of the structure by heating and consequent adsorption of water to the active surface. The bending vibration at 1762.7 cm^{-1} shows an additional peak due to adsorbed water. The IR analysis of A10Z and A15Z samples shows the disappearance of peaks at 3656 cm^{-1} (due to the stretching vibration of physically adsorbed –OH with Al^{3+}) and 3552 cm^{-1} (due to the stretching vibration of physically adsorbed –OH with Zr^{4+}) after

Table 3
Particle size analysis of A15Z powder calcined at 1000 °C for 2 h

	Volume statistics, size (μm)
D_{10}	0.027
D_{25}	0.045
D_{50}	0.11
D_{75}	0.175
D_{90}	0.229
Mean	0.127

calcination at 200 °C. The disappearance of peaks corresponding to adsorbed water in A15Z sample could be related to the reduction in surface positive charge density of Al_2O_3–ZrO_2 system with the increase in ZrO_2 content. The –OH group bonded with Al^{3+} shows a peak at 3447.9 cm^{-1} with the corresponding bending vibrations at 1638.2 and 1385.3 cm^{-1} (Fig. 2b). Bending vibration and/or coupled vibration of –OH group attached with Zr^{4+} disappeared at this temperature.

After calcination at 400 °C, for A5Z batch, all the peaks related to stretching vibration of free and bonded water disappear. Only one peak at 3461 cm^{-1} still exists, which is related to the stretching vibration of –OH group attached with Al^{3+}. Bending vibration and/or coupled vibration of Al–OH group can only be observed in the spectrogram. On the lower frequency side a peak at 596.7 cm^{-1} is observed which could be related to the Al–O vibration. Heating at 400 °C causes broadening of peaks in the lower frequency range (500–1000 cm^{-1}) due to overlapping of Al–O and Zr–O infrared vibrations of transition alumina and zirconia phases. Thus, individual peaks corresponding to Zr–O could not be detected in the temperature range 200–400 °C. However, at higher temperature (1000 °C) peaks corresponding to Al–O and Zr–O could be clearly observed. Similar trend is also followed in A75Z, A10Z and A15Z samples.

IR spectra shows that a trace amount of –OH group still remains in the structure of ZrO_2 dispersed Al_2O_3 powder even after heating at 1000 °C. The reduced intensity of –OH absorption band could be due to the moisture absorption during testing. A10Z powder calcined at 1000 °C shows a peak at 3484.3 cm^{-1} corresponding to Al–OH stretching vibration. The stretching of crystalline Al–O and Zr–O bonds show absorption bands at lower frequencies of 828.0 and 525.6 cm^{-1}, respectively, for A15Z samples [19].

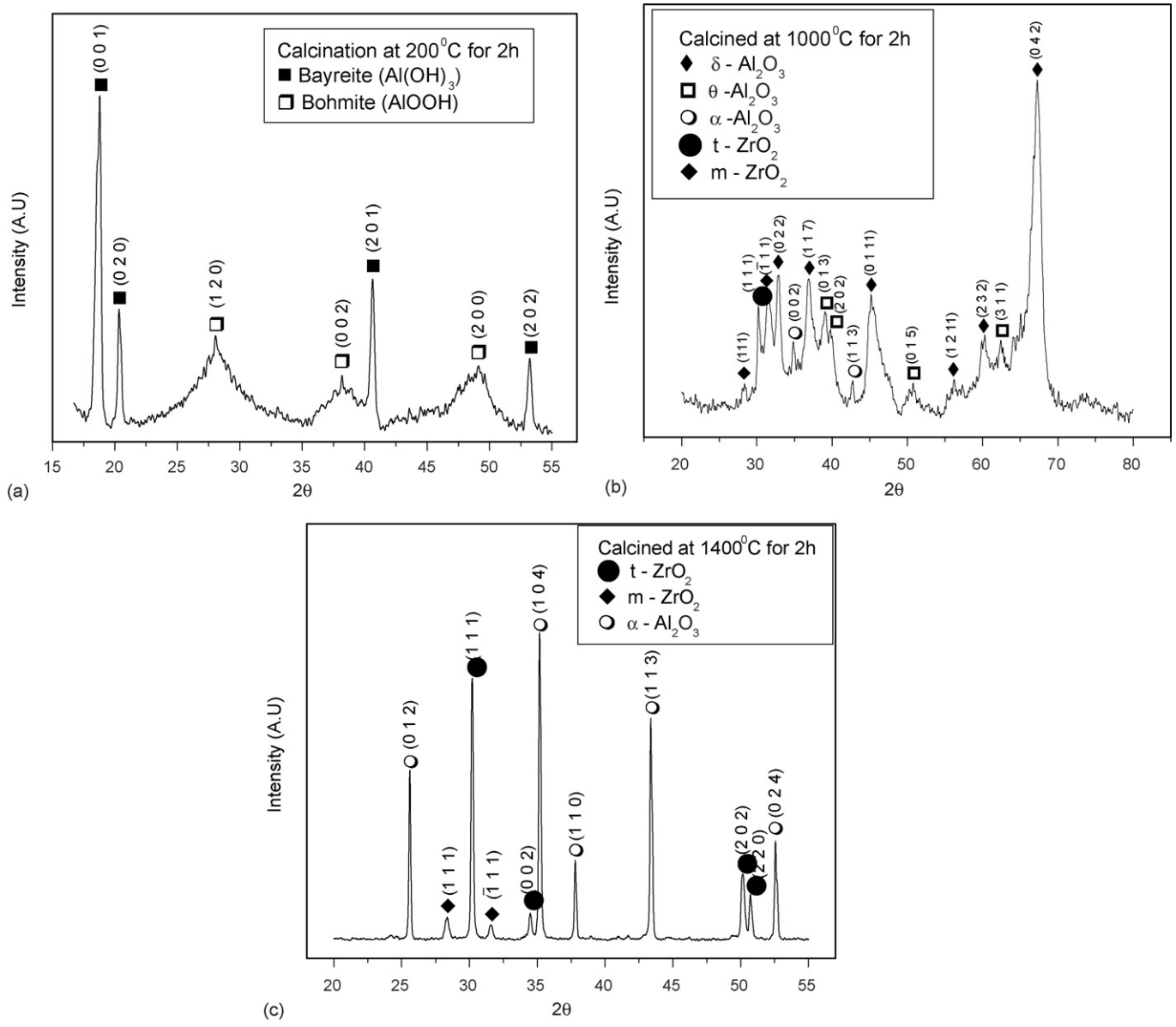

Fig. 3. Phase analysis of Al_2O_3–$15ZrO_2$ (mol%) powders calcined at (a) 200 °C for 2 h, (b) 1000 °C for 2 h and (c) 1400 °C for 2 h.

3.2. XRD analysis

The sequence of phase evaluation in the calcined A15Z hydrogel was studied by XRD. The XRD pattern of the as-dried gel (Fig. 3) shows broad peak of bayerite only. The broad peak of bayerite indicates the presence of fine crystallites (crystallite size 5–20 nm). XRD of hydrogel calcined at 200 °C have both bayerite ($Al(OH)_3$) and boehmite (Al(O)OH). Boehmite crystallizes from bayerite on heating according to the reaction:

$$Al(OH)_3 = Al(O)OH + H_2O \quad (2)$$

The IR analysis of hydrogel also confirms the presence of intermediate boehmite as well as Zr–O bond of non-crystalline zirconia (Fig. 2a). Calcination at higher temperature (1000 °C) induces further phase transition in boehmite as well as crystallization of zirconia from amorphous zirconium hydroxide (Fig. 3b). At this temperature, the following phases were identified m-ZrO_2, t-ZrO_2, δ-Al_2O_3, θ-Al_2O_3 and α-Al_2O_3. The crystallite size of the calcined powder at 1000 °C for 2 h is in the range of 20–160 nm. Usually α-Al_2O_3 crystallizes around 1200 °C, however, in the present study the lower crystallization temperature of α-Al_2O_3 could be related to the fine crystallite size and higher specific surface area. The phases present at the highest treatment temperature (1400 °C) are α-Al_2O_3, t-ZrO_2 and m-ZrO_2 (Fig. 3c). The increase in m-ZrO_2 content at 1400 °C results from an increase in the grain size of zirconia, which induces partial t–m transformation during cooling. Thus, XRD analysis of A15Z emphasizes that the phase transformation from bayerite to α-Al_2O_3 agrees well with earlier studies [20]. The reduction of specific volume to the extent of 24% is observed during phase transformation of boehmite (0.332 cm^3/g) to α-Al_2O_3 (0.251 cm^3/g), probably results in the generation of intraparticle porosity in the alumina particles [21].

3.3. Thermal behavior of hydrogel

The DTA–TG curve of the dried A15Z gel powder is shown in Fig. 4. In the temperature range 50–300 °C DTA curve shows a broad endothermic peak at 110 °C, a sharp exothermic peak at about 225 °C and another endothermic peak at 280 °C. At higher temperature, the DTA curve shows a sharp and a small exothermic peak at about 420 °C, a sharp but small endothermic peak at about 480 °C. Finally, the DTA curve shows a small exothermic peak at about 1160 °C. The TG curve of the gel shows a gradual weight loss of about 15% in the temperature range 25–210 °C and a sharp weight loss of about 18% in the temperature range 210–315 °C show a further weight loss of about 17% which takes place in three stages. The first stage of this weight loss is about 5% in the temperature range 315–320 °C, the second stage about 10% in the temperature range 320–455 °C and the final stage of weight loss is about 2.0% in the temperature range 455–545 °C.

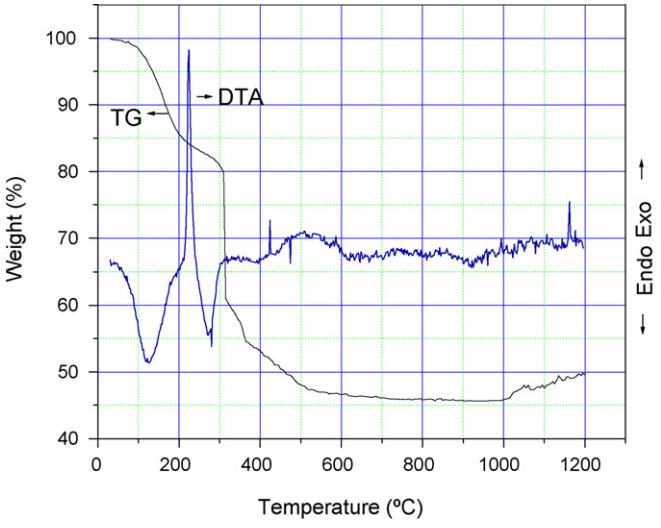

Fig. 4. TG/DTA plot for the Al_2O_3–$15ZrO_2$ (mol%) precursor powders in air.

The above thermal behavior of the A15Z gel powder could be explained according to following: the gel powder contains disordered pseudoboehmite at room temperature having more than 15% excess water in its lattice [22]. The theoretical weight loss due to dehydroxylation of pseudoboehmite is about 13% for A15Z sample which matches well with the observed weight loss. Thus, the first endothermic peak and the associated weight loss correspond to the dehydroxylation of pseudoboehmite. The dehydroxylation of pseudoboehmite is associated with the crystallization of bayerite (β-$Al_2O_3{\cdot}3H_2O$). Thus, the exothermic peak could be related to the crystallization of bayerite. The bayerite thus formed undergoes further dehydroxylation to boehmite (α-AlOOH) in the temperature range 280–308 °C. The theoretical weight loss for this reaction is 19.61%. The observed weight loss 19% agrees well with this transformation. Subsequently, boehmite changes to γ-$Al2O_3$ according to the reaction:

$$2AlO(OH) = Al_2O_3 + H_2O \quad (3)$$

The theoretical weight loss is 15% and for A15Z this will be 12.75%. The observed weight loss agrees well with the theoretical loss. The weight loss is associated with one exothermic and one endothermic peak. The presence of these peaks could be explained as follows: AlO(OH) does not transform to γ-Al_2O_3 directly. Literature reviewed says that AlO(OH) first transforms to an amorphous alumina on dehydroxylation which subsequently crystallizes to γ-Al_2O_3 [23]. Thus, the exothermic and endothermic peaks in the temperature range 415–480 °C corresponds to the conversion of dehydroxylated boehmite to γ-Al_2O_3 via the intermediate step of amorphous alumina. Finally the exothermic peak at 1160 °C corresponds to crystallization of α-Al_2O_3. However, X-ray diffractograms of powders calcined for 2 h at 1000 °C show the presence of α-Al_2O_3. The difference in crystallization temperature of α-Al_2O_3 as observed in DTA and XRD could be because of the difference in heating schedule for the two samples. While X-ray pattern was recorded on samples which were held for 2 h at 1000 °C, the DTA was done without any isothermal hold. Thus, the isothermal hold at 1000 °C has accelerated the transformation to α-Al_2O_3 at lower temperature. Similar change in the crystallization temperature of α-Al_2O_3 was also observed by the same research group in an earlier work [24].

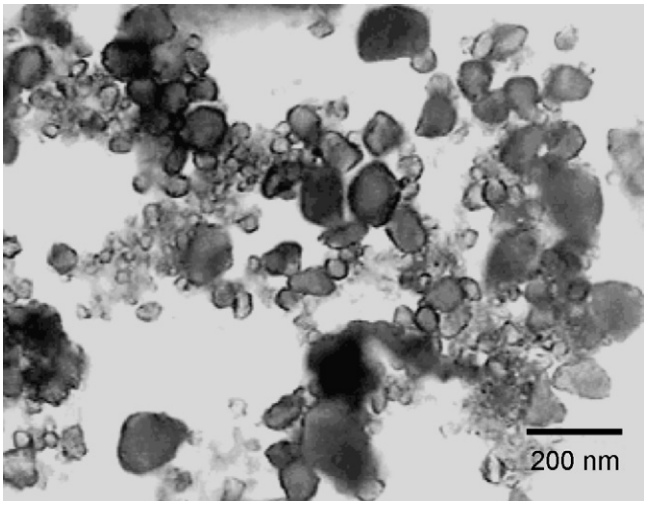

Fig. 5. TEM photograph of 15 mol% ZrO_2 doped Al_2O_3 powder. Precursor powder was calcined at 1000 °C for 2 h.

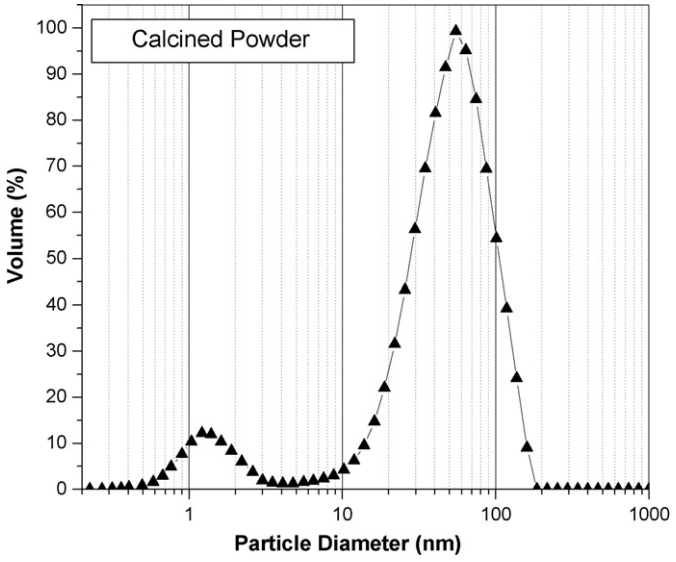

Fig. 6. Particle size analysis of calcined powder at 1000 °C for 2 h.

On the other hand, the transformation of $Zr(OH)_4$ to ZrO_2 follows the reaction [25]:

$$Zr(OH)_4 = ZrO_{1.5}(OH) + 1.5H_2O \quad (4)$$

$$ZrO_{1.5}(OH) = ZrO_2 + 0.5H_2O \quad (5)$$

The theoretical weight loss for the dehydroxylation of $Zr(OH)_4$ and its crystallization to ZrO_2 following the above reaction sequence of Eqs. (3) and (4) should be about 4%. The observed weight loss matches well with the theoretical value.

3.4. TEM analysis

The TEM micrographs (Fig. 5) show uniform distribution of fine sized particles (light shade) in the range (≤20 nm). Thus, the prepared powder was in the nanometer range. The micrograph also shows a number of dark patches (about 100–180 nm) which indicate the agglomerated particles cluster which probably have resulted during sample preparation. The particle size analysis (Fig. 6) of the calcined powder also shows that the particles have a bimodal size distribution. The finer particle (≤20 nm) represents the unagglomerated particles while the larger size particle (60–180 nm) represents the agglomerate size. The measured BET specific surface area of the calcined powder (1000 °C for 2 h) was found to be 130 m^2/g. The surface area data could be utilized to indirectly determine the particle size of the powder using the equation [26]:

$$D = \frac{6}{\rho S}$$

where D is the particle size, ρ the theoretical density of the powder and S is the specific area.

Assuming the particles to be spherical in nature and the theoretical density of A15Z to be 4.28 g/cm^3 the calculated particle size was found to be ~10 nm. Thus, the calculated particle size agrees well with the particle size measured from TEM photograph.

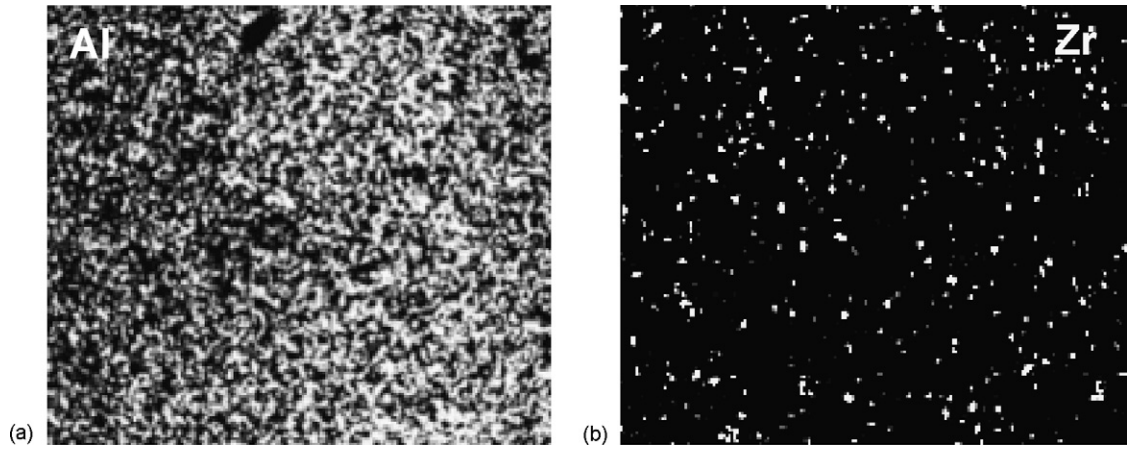

Fig. 7. X-ray mapping micrographs of different elements: (a) Al and (b) Zr of sintered and polished surface.

3.5. EPMA

The X-ray mapping (EPMA analysis) of polished and thermally etched surface showing the presence of different elements (Al and Zr) within the matrix is illustrated in Fig. 7. The Zr mapping (Fig. 7b) shows an almost uniform distribution of ZrO_2 in the alumina matrix. However, considering the size and distribution of Zr X-ray mapping, it may be inferred that some zirconia particles are in an agglomerated state, although the volume fraction of agglomerated zirconia is less. This homogeneous distribution assists to enhancement of the thermo-mechanical properties [27]. Thus, it can be inferred that the distribution of zirconia in the sintered samples remains unaltered with increasing zirconia content. The near homogenous distribution of alumina and zirconia in the sintered samples of both A5Z as well as A15Z samples indicate that alumina and zirconia were uniformly distributed in the sintered samples as well as calcined powders of all the compositions studied. This homogenous distribution of alumina and zirconia is due to homogeneous particle size distribution of the starting powders.

4. Conclusions

This present study on the characterization of sol–gel derived amorphous ZTA powder led to the following conclusions:

(a) The decomposition and crystallization of pseudoboehmite to γ-Al_2O_3 occurred in three-stages. The transition from γ-Al_2O_3 to α-Al_2O_3 followed the intermediate stage of θ-Al_2O_3 formation. On the other hand, t-ZrO_2 crystallization from $Zr(OH)_4$ in single stage.
(b) FTIR study suggests the presence of both four and six coordinated Al while Zr was four coordinated. The number and intensity of M–OH and M–O bonds increase on increasing ZrO_2 content.
(c) TEM image shows the presence of nano-sized particles (∼20 nm) along with a few particle clusters of about 180 nm. The particle clusters resulted from agglomeration.
(d) EPMA picture shows that ZrO_2 particles are near uniformly distributed in the matrix.
(e) Particle size distribution indicates a bimodal size distribution with higher particle size distribution around 180 nm. Thus, the size distribution indicates both unagglomerated and agglomerated particles.

References

[1] K. Wefers, C. Misra, Oxides and hydroxides of aluminium, Alcoa Technical Paper No. 19, Alcoa Laboratories, Pittsburgh, PA, 1987.
[2] W.A. Yarbrough, R. Roy, Microstructural evolution in sintering of AlOOH gels, J. Mater. Res. 2 (4) (1987) 494–515.
[3] P.F. Becher, B.K. Alexander, A. Bleier, B.S. Waters, W.H. Warwick, Influence of ZrO_2 grain size and content on the transformation response in the Al_2O_3–ZrO_2 (12 mol%CeO_2) system, J. Am. Ceram. Soc. 76 (3) (1993) 657–663.
[4] B. Basu, J. Vleugels, O. Van Der Biest, Transformation behaviour of tetragonal zirconia: role of dopant content and distribution, Mater. Sci. Eng. A 366 (2) (2004) 338–347.
[5] T. Venkateswaran, D. Sarkar, B. Basu, Tribological properties of WC–ZrO_2 nanocomposites, J. Am. Ceram. Soc. 88 (3) (2005) 691–697.
[6] S. Hori, M. Yoshimura, S. Somiya, Al_2O_3–ZrO_2 ceramics prepared from CVD powders, in: N. Claussen, A.H. Heuer, M. Rühle (Eds.), Advances in Ceramics, vol. 12, The American Ceramic Society, Columbus, OH, 1984, pp. 794–805.
[7] D.W. Sproson, G.L. Messing, Preparation of alumina–zirconia powders by evaporation decomposition of solutions, J. Am. Ceram. Soc. 67 (5) (1984) C92–C93.
[8] I.A. Aksay, F.F. Lange, B.I. Davis, Uniformity of Al_2O_3–ZrO_2 composites by colloidal filtration, J. Am. Ceram. Soc. 66 (10) (1983) C190–C192.
[9] Y. Wu, A. Bandyopadhyay, S. Bose, Processing of alumina and zirconia nano-powders and compacts, Mater. Sci. Eng. A 380 (2004) 349–355.
[10] M. Kagawa, M. Kikuchi, Y.N. Syono, Stability of ultrafine tetragonal ZrO_2 coprecipitated with Al_2O_3 by the spray-ICP technique, J. Am. Ceram. Soc. 66 (11) (1983) 751–754.
[11] K. Matusi, M. Ohgai, Formation mechanism of hydrous zirconia particles produced by hydrolysis of $ZrOCl_2$ solutions. IV. Effects of $ZrOCl_2$ concentration and reaction temperature, J. Am. Ceram. Soc. 85 (3) (2002) 545–553.
[12] J.A. Navio, G. Colón, P.J. Sáachez-soto, M. Macias, Chem. Mater. 9 (1997) 1256–1261.
[13] M.C. Caracoche, P.C. Rivas, M.M. Cervera, R. Caruso, E. Benavádez, O. de Sanctís, S.R. Mintzer, J. Mater. Res. 18 (2003) 208–215.
[14] S.G. Chen, Y.S. Yin, D.P. Wang, Experimental and theoretical investigation on the correlation between aqueous precursors structure and crystalline phases of zirconia, J. Mol. Struct. 690 (2004) 181–187.
[15] N.N. Greenwood, A. Earnshaw, Chemistry of the Elements, 2nd ed., Butterworth-Heinemann, Oxford, 1997.
[16] R.I. Zakharchenya, T.N. Vasilevskaya, J. Mater. Sci. 29 (1994) 2806.
[17] G.Y. Guo, Y.L. Chen, High-quality zirconia powder resulting from the attempted separation of acetic acid from acrylic acid with zirconium oxychloride, J. Mater. Chem. 11 (2001) 1283–1287.
[18] Ph. Colomban, Structure of oxide gels and glasses by infrared and Raman scattering, J. Mater. Sci. 24 (1989) 3002–3010.
[19] M. Low, R. McPherson, Crystallization of gel-derived alumina and alumina–zirconia ceramics, J. Mater. Sci. 24 (1989) 892–898.
[20] H.Y. Lee, R. Werner, B.L. Mordike, Sintering of nanocrystalline ZrO_2 toughened alumina (ZTA) and zirconia, J. Eur. Ceram. Soc. 10 (1992) 245–253.
[21] B.B. Roger, G.L. Messing, Effect of seeding and water vapor on the nucleation and growth of alpha-Al_2O_3 from gamma-Al_2O_3, J. Am. Ceram. Soc. 82 (1999) 825.
[22] I. Levin, D. Brandon, Metastable alumina polymorphs: crystal structures and transition sequences, J. Am. Ceram. Soc. 81 (8) (1998) 1995–2012.
[23] Determination of the structure of γ-alumina using empirical and first principles calculations combined with supporting experiments, Ph.D. Dissertation by Gianluca Paglia, Curtin Univeristy of Technology, Australia, 2004.
[24] S. Bhattacharyya, S. Bharati, S.K. Pratihar, R.K. Sinha, R.C. Behera, R.I. Ganguly, Sintering behavior of Al_2O_3–ZrO_2 microcomposites prepared by a combined gel–precipitation route, Trans. Indian Ceram. Soc. 62 (1) (2003) 18–21.
[25] A. Clearfield, G.H. Nancollas, R.H. Blessing, in: J.A. Marinsky, Y. Marcus (Eds.), Ion Exchange and Solvent Extraction, vol. 5, Marcel Dekker, New York, 1973.
[26] M.N. Rahaman, Ceramic Processing and Sintering, Marcel Dekker, Inc., New York, 1995, 115 pp.
[27] D. Sarkar, S. Adak, S.J. Cho, M.C. Chu, N.K. Mitra, Influence of ZrO_2 content and grain size on the thermo-mechanical properties of nano-ZTA, Ceram. Int. 33 (2007) 255–261.